AIP | Journal of Applied Physics

Ab initio modeling of zincblende AlN layer in Al-AlN-TiN multilayers

S. K. Yadav, J. Wang, and X.-Y. Liu

Citation: Journal of Applied Physics **119**, 224304 (2016); doi: 10.1063/1.4953593
View online: http://dx.doi.org/10.1063/1.4953593
View Table of Contents: http://scitation.aip.org/content/aip/journal/jap/119/22?ver=pdfcov
Published by the AIP Publishing

Ab initio modeling of zincblende AlN layer in Al-AlN-TiN multilayers

S. K. Yadav,[1,a)] J. Wang,[2] and X.-Y. Liu[1,a)]
[1]*Materials Science and Technology Division, MST-8, Los Alamos National Laboratory, Los Alamos, New Mexico 87545, USA*
[2]*Mechanical and Materials Engineering, University of Nebraska-Lincoln, Lincoln, Nebraska 68588, USA*

(Received 22 March 2016; accepted 27 May 2016; published online 13 June 2016)

An unusual growth mechanism of metastable zincblende AlN thin film by diffusion of nitrogen atoms into Al lattice is established. Using first-principles density functional theory, we studied the possibility of thermodynamic stability of AlN as a zincblende phase due to epitaxial strains and interface effect, which fails to explain the formation of zincblende AlN. We then compared the formation energetics of rocksalt and zincblende AlN in fcc Al through direct diffusion of nitrogen atoms to Al octahedral and tetrahedral interstitials. The formation of a zincblende AlN thin film is determined to be a kinetically driven process, not a thermodynamically driven process. *Published by AIP Publishing*. [http://dx.doi.org/10.1063/1.4953593]

I. INTRODUCTION

Aluminum nitride (AlN) is a wide-gap optoelectronic material that is of considerable technology interest,[1] with many unique properties such as relatively high hardness, high thermal conductivity, etc. AlN thin films have also been grown on various substrates for application such as piezoelectric material.[2,3] The ground state equilibrium structure of AlN at ambient temperature and pressure is B4 type, hexagonal wurtzite (*wz*-AlN). Additionally, AlN can also exist as a metastable B3 type, cubic zincblende structure (*zb*-AlN) or the high-pressure B1 type, cubic rock-salt variant (*rs*-AlN), as predicted using density functional theory (DFT) calculations.[4–6]

There has been a growing interest in the metastable cubic films of AlN recently, aiming to achieve novel and enhanced mechanical and functional properties that are not observed in the hexagonal structure. By tailoring substrates in terms of crystal structure, substrate orientation, and elastic mismatch, the cubic crystal structure of AlN layers can be grown in superlattice systems and the stability of the cubic structures strongly depends on their layer thickness. At an annealing temperature of 600 °C, epitaxial metastable *zb*-AlN was synthesized by the solid-state reaction between single crystal Al(001) and TiN(001).[7] In magnetron sputtering deposited AlN/TiN(001) epitaxial superlattices, the high-pressure *rs*-AlN was stabilized with AlN layer thickness less than or equal to 2.0 nm.[1] Using reactive sputtering, the epitaxial stabilization of *rs*-AlN was also observed in AlN/VN(001) and AlN/TiN(001) superlattices with critical layer thickness of AlN before transforming to *wz*-AlN, 3 to >4 nm and 2–2.5 nm, respectively.[8,9] The stabilization of *zb*-AlN was also observed in AlN/W(001) superlattices with the AlN thicknesses less or equal to 1.5 nm.[10]

Recent *ab initio* study shows that at ambient temperature and pressure, the most stable phase of AlN is the hexagonal wurtzite structure, while at high pressures and temperatures the rock-salt phase becomes more stable.[6] Zincblende phase was not found to be stable at any combination of pressure and temperature. This rules out the possibility of temperature or pressure playing a role in the formation of zincblende AlN.[6] DFT based calculations have also been employed before to investigate the formation and stability of the (100) AlN/TiN, AlN/VN, and VN/TiN in the rock-salt structure.[11] More recently, first-principles molecular dynamics have been used to investigate the thermal and mechanical stability of the (100) Ti/AlN rock-salt structure, with one or two monolayers of AlN as interfacial layers.[12]

In a recent experimental work, using reactive direct current magnetron sputtering, thin multilayers of alternating Al-AlN-TiN layers were deposited at room temperature.[13] The diffraction pattern confirms the orientation relation between the Al and the TiN layers, $(111)_{Al}||(111)_{TiN}||$ interface and $\langle 110\rangle_{Al}||\langle 110\rangle_{TiN}$, and the growth direction is along [111]. The AlN layer is about 1.5 nm thick and adopts *zb*-AlN.[13] After the indentation testing, the *zb*-AlN layer gradually transforms into the *wz*-AlN layer.[13] In Figures 1(a)–1(c), schematics of growth process and indentation are shown. The most intriguing findings are the growth of metastable *zb*-AlN layers only on top of the Al layer and the *zb*-AlN to *wz*-AlN transformation after mechanical loading. In this paper, details of DFT calculations

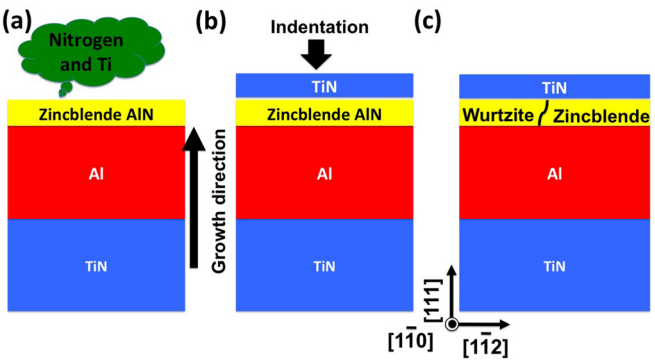

FIG. 1. The schematic of Al-AlN-TiN trilayer growth. (a) Al layer is exposed to nitrogen and titanium. (b) and (c) This leads to the formation of *zb*-AlN and TiN layer. Under uniaxial indentation, *zb*-AlN partially transforms to *wz*-AlN.[13]

[a)]Authors to whom correspondence should be addressed. Electronic addresses: syadav@lanl.gov, yadav.satyesh@gmail.com, and xyliu@lanl.gov

TABLE I. Comparison of calculated and available experimental values of lattice parameters, bulk modulus, of Al, TiN, and AlN in wurtzite (*wz*), zincblende (*zb*), and rock-salt (*rs*) phases.

	Al		*wz*-AlN		*zb*-AlN	*rs*-AlN	TiN	
	DFT	Exp.	DFT	Exp.	DFT	DFT	DFT	Exp.
Lattice parameter (Å)	4.04	4.05[20]	3.12 (a) 5.01 (c)	3.11 (a)[21] 4.98 (c)[21]	4.40	4.06	4.24	4.24[22]
Bulk modulus (GPa)	76	79[23]	202	211[24] 208[25] 220[26]	224	298	306	318[27]
Relative energy (meV/f.u.)			0.0		43	345		

are presented, providing a theoretical basis to understand the energetics involved in the formation of *zb*-AlN layer as well as for phase transformation during mechanical loading.

The rest of this paper is organized as follows. The computational methods along with descriptions of the structural models are provided in Sec. II. For presenting DFT results in Sec. III, we started with exploring the possibility of stabilizing AlN in the zincblende phase due to various types of strains introduced during growth. Then, we considered the interfaces between Al/AlN and AlN/TiN as possible sources that may thermodynamically stabilize the zincblende phase. Finally, we demonstrated that the kinetically driven diffusion of nitrogen is the only feasible explanation of the zincblende AlN formation.

II. METHODS

Our DFT calculations were performed using the Vienna *Ab initio* Simulation Package (VASP).[14,15] The DFT calculations employed the Perdew, Burke, and Ernzerhof (PBE)[16] generalized gradient approximation (GGA) exchange-correlation functional and the projector-augmented wave (PAW) method.[17] For all calculations, a plane wave cutoff of 500 eV for the plane wave expansion of the wave functions was used to obtain highly accurate forces. $12 \times 12 \times 12$, $7 \times 7 \times 7$, $3 \times 3 \times 3$, $3 \times 3 \times 3$, and $3 \times 3 \times 5$ Monkhorst-pack meshes for k-point sampling are required to calculate the elastic constants of Al, TiN, zb-AlN, rs-AlN, and wz-AlN phases, respectively. All structures are considered converged when each component of the force on every atom is smaller than 0.02 eV/Å. The numbers of valence electrons in the pseudo-potentials are 3 ($2s^2$, $2p^1$) for Al, 5 ($2s^2$, $2p^3$) for N, and 10 ($3p^6$ $4s^2$ $3d^2$) for Ti. Table I lists the DFT calculated values and available experimental values of lattice parameters, bulk modulus of Al, and AlN in *wz*-AlN, *zb*-AlN, and *rs*-AlN phases, and TiN in the rock-salt crystal structure. Bulk moduli were determined from the energy vs. volume curve using Birch-Murnaghan equation of state. The agreement between the DFT values and the experimental data is excellent.[18,19] The relative energies of various phases of AlN per formula unit are also listed. From Table I, it is shown that the wurtzite phase is most energetically stable, while the zincblende phase is 43 meV higher than the wurtzite phase, and the rocksalt phase is 345 meV higher.

Interface calculations involve supercells of slabs periodically repeating in the interface plane and a vacuum region of more than 12 Å normal to the interface plane to avoid surface-surface interactions. A dipole correction perpendicular to the interface is added if both terminating surfaces are not metallic.[28] A $7 \times 7 \times 1$ Monkhorst-Pack mesh for k-point sampling is used for all calculations involving interfaces, with 1 k-point along the largest length in the simulations. In-plane lattice parameters corresponding to the equilibrium lattice parameter of TiN and *zb*-AlN are considered. Similar methodology has been applied to our earlier metal/nitride interface calculations.[18,29,30]

III. RESULTS AND DISCUSSION

A. Various phases of bulk AlN under stress

During the growth and later under indentations, AlN may experience various types of stresses. As AlN has interfaces with TiN and Al in the (111) plane, so we considered three types of stresses that best represent the structural constraints: (1) hydrostatic stress, (2) biaxial stress in (111) plane, and (3) uniaxial stress along [111] direction. Figure 2 shows supercells of various crystal structures used to study the effect of various types of stresses.

For hydrostatic stress effect, we calculated the relative formation energies (equilibrium *zb*-AlN formation energy is taken as reference) of the wurtzite, the zincblende, and the rocksalt structures as a function of volume (per formula unit) as shown in Figure 3(a). For all ranges of hydrostatic stress considered, the wurtzite phase is lower in energy compared to the zincblende phase. Under large compressive stress, the wurtzite phase transforms to the rock-salt phase, which was also predicted by the previous calculations.[6] The *wz*-AlN to the *rs*-AlN phase transformation is accompanied by a

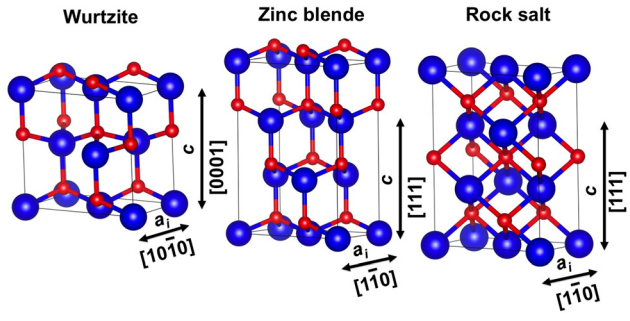

FIG. 2. Supercells of various crystal structures and definition of lattice parameters a_i and c.

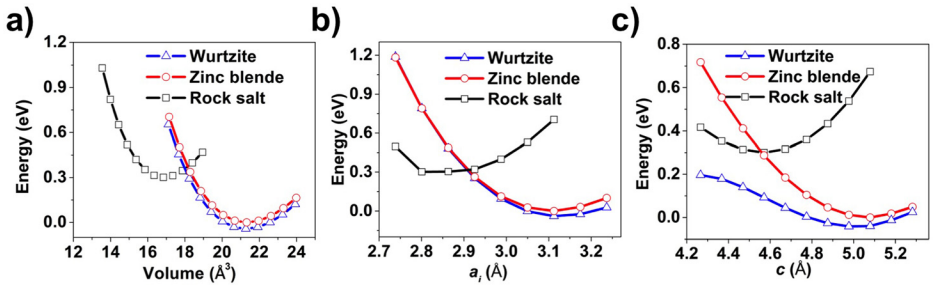

FIG. 3. Relative formation energy (equilibrium *zb*-AlN formation energy is taken as reference) per formula unit under (a) hydrostatic stress as a function of crystal volume (per formula unit), (b) biaxial stress as a function of lattice parameter a_i, and (c) uniaxial stress as function of lattice parameter *c*.

volume reduction of 20.5% which is in good agreement with experimental values of 20.6%[31] and 18%[3] and theoretical values of 19%[4] and 22.5.[32]

As AlN interfaces with both Al and TiN, it experiences biaxial stress in the (111) plane. Fig. 3(b) shows the relative formation energy (equilibrium *zb*-AlN formation energy is taken as reference) per formula unit as a function of lattice parameter a_i. To make lattice parameter consistent for all phases, a_i is *defined as* the distance between two nearest Al atoms, as shown in Fig. 2. For wurtzite crystal structure, a_i equals to the hexagonal lattice parameter a_0. For the *wz*-AlN and the *zb*-AlN, a_i equals to $a_0/\sqrt{2}$, where a_0 is the cubic lattice constant. As biaxial strain is introduced in the (111) plane, the lattice normal to the plane is allowed to relax so that there is no stress in [111] direction. As the in-plane lattice parameters of *wz*-AlN and *zb*-AlN become smaller, the relative energy between the two compounds decreases. However, at no point the *zb*-AlN becomes more stable than the *wz*-AlN. In addition, at in-plane lattice parameter a_i of 2.9 Å, *rs*-AlN becomes more stable than both the *wz*-AlN and the *zb*-AlN (see Fig. 3(b)).

When the Al/AlN/TiN stack is indented in the [111] direction, AlN may experience uniaxial stress in the [111] direction. We calculated the relative formation energy (equilibrium *zb*-AlN formation energy is taken as reference) as a function of lattice parameter *c*. To make comparison between different crystal structures easy, we again define lattice parameter *c* for the zincblende and the rock-salt as 2/3 of $a_{[111]}$ or $2\sqrt{3}/3$ a_0, where a_0 is the cubic lattice constant, as shown in Fig. 2. For the wurtzite crystal structure, *c* equals to the hexagonal lattice parameter c_0 in [0001]. This is justified, as *c* represents two stacks (AB) of Al atoms from ABABAB stacking in the wurtzite phase or ABCABCABC stacking in the zincblende and the rocksalt phases.

Under uniaxial stresses, as the lattice is strained along the [111] direction, the lattice parameters in the (111) plane are allowed to relax so that there is no stress in the same plane. As shown in Fig. 3(c), under uniaxial compressive stresses, the difference in energy between the wurtzite phase and the zincblende phase becomes larger as the stress increases, with the wurtzite phase more stable than the zincblende phase. This explains the tendency of the zincblende phase transforming to wurtzite under uniaxial compressive stress. However, under uniaxial compressive stress considered, the energy of the rock-salt phase is always higher than that of the wurtzite phase.

Various types of stresses that might arise during the growth do not explain the stabilization of the zincblende phase. Next, we explore the possibility of the zincblende phase stabilization due to the interfaces in Al/AlN/TiN multilayers.

B. Energetics of Al/AlN and AlN/TiN bilayers

We started by exploring the relative stability of Al/AlN and AlN/TiN interfaces when AlN is in the zincblende versus the wurtzite phases. In-plane lattice parameters can take several values. Here, for all calculations, we have constrained the in-plane lattice parameters to that of *zb*-AlN. It is worth pointing out that there are several different configurations of interfaces due to the different terminations of *wz*-AlN and *zb*-AlN. We will first discuss these different terminations. In normal growth conditions, nitrogen atoms are expected to be the terminating species at the interface, as suggested in our earlier works.[29] Fig. 4(a) shows ABABA stacking of *wz*-AlN and one dangling bond (1*db)* and three dangling bonds (3*db)* termination of the nitrogen layer of AlN. Similarly, Fig. 4(b) shows ABCAB stacking of *zb*-AlN and two possible nitrogen terminations of AlN: 1*db* and 3*db*. Thus, AlN interfaced with either Al or TiN can form several types of interfaces.

We first studied various possible interfaces between Al/AlN. Here, we only discuss the interfaces with the most stable interface structures found in terms of interface shifts relative to the bicrystals. As mentioned earlier, there are two possible terminations of AlN in both phases, with the nitrogen layer terminating in one dangling bond 1*db* and three dangling bonds 3*db*. As shown in Figures 5(a) and 5(b), we note that the stacking sequence of AlN for both *wz*-AlN and

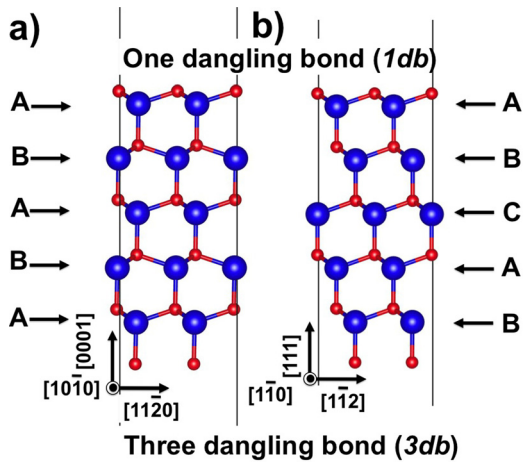

FIG. 4. Atomic structure of stacking sequence and termination of (a) left, *wz*-AlN and (b) right, *zb*-AlN.

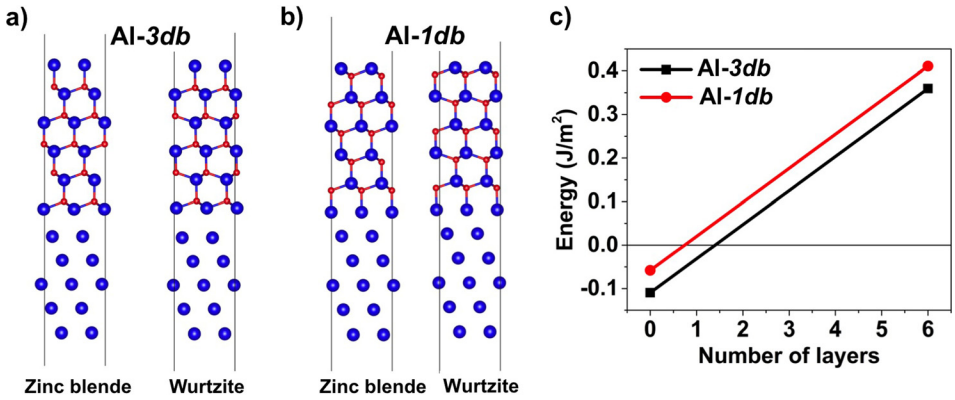

FIG. 5. Atomic structure of Al/AlN slabs (a) Al-3*db* and (b) Al-1*db*. (c) Relative stability of *zb*-AlN with respect to *wz*-AlN as a function of number of layers.

zb-AlN is the same near the interface (AB). Moreover, nitrogen atoms are located at the natural positions of each lattice type involved. As it is not possible to calculate the absolute free surface or interface energy of AlN, we calculated the relative interface energy when AlN is in the zincblende versus in the wurtzite phases. We assumed that the surface energies of the terminating surfaces of *wz*-AlN and *zb*-AlN are the same, which have been practiced by earlier work.[33] To calculate the relative interface energy, the total energy of the system (E_{slab}) is partitioned into bulk energies, surface energies, and interface energies

$$E_{int}^{Energy} = (E_{Slab}^{zb/wz} - nE_{Bulk}^{zb/wz})/A - S^{Al} - S^{zb/wz}, \quad (1)$$

then the relative interface energy is

$$E_{\mathbf{int}}^{rel} = \frac{E_{slab}^{zb} - E_{slab}^{wz} - n\left(E_{bulk}^{zb} - E_{bulk}^{wz}\right)}{A}, \quad (2)$$

where E_{slab}^{zb} and E_{slab}^{wz} are the slab energies having *zb*-AlN and *wz*-AlN, respectively. E_{bulk}^{zb} and E_{bulk}^{wz} are the bulk energies of *zb*-AlN and *wz*-AlN; n is the number of formula unit of AlN; and *A* is the interface area. In this work, we did not consider interface interactions. This is equivalent to assuming that the number of AlN layers does not affect the relative interface energy. We also calculated the relative formation energy as a function of number of layers of AlN, h_n,

$$E_f^{rel} = E_{\mathbf{int}}^{rel} + \frac{2h_n\left(E_{bulk}^{zb} - E_{bulk}^{wz}\right)}{A}. \quad (3)$$

Figure 5(c) plots the excess relative energy of *zb*-AlN with respect to *wz*-AlN as a function of number of AlN layers. There are approximately 6 layers of *zb*-AlN layers during the growth in experimental conditions but interface alone only stabilizes 1–1.5 layers. The structure of AlN/TiN interface is similar to that of Al/TiN interface, with preference for AB stacking as shown in Figs. 6(a) and 6(b). Figure 6(c) plots the excess energy of *zb*-AlN with respect to *wz*-AlN as a function of number of AlN layers. The interface alone only stabilizes up to two layers of *zb*-AlN.

C. Energetics of Al/AlN/TiN multilayers

In Sec. III B, we established the most stable terminations and configurations for Al/AlN interface and AlN/TiN interface. Here, we calculate the relative interface energy with both Al/AlN and AlN/TiN interfaces in the same supercell. There are two possible combinations for *wz*-AlN and *zb*-AlN interfaced with Al on the one side and TiN on the other side, as shown in Figs. 7(a) and 7(b). In the first configuration while Al forms 3-*db* bond with the N layer of AlN, TiN forms 1-*db* bond. In the second configuration while TiN forms 3-*db* bond with the N layer of AlN, Al forms 1-*db* bond. In order to calculate the relative interface formation and relative formation energies, Eqs. (2) and (3) are applied, respectively. Fig. 7(c) shows the relative formation energies of two configurations as a function of number of AlN layers. For all configurations considered, the maximum number of *zb*-AlN layers that interfaces can stabilize is about two, which is about 0.5 nm thickness. The change in the (111) in-plane lattice parameters does not significantly change the relative formation energy.

Intuitively, the interface energy of Al/AlN/TiN multilayers should be equal to the sum of the interface energies of

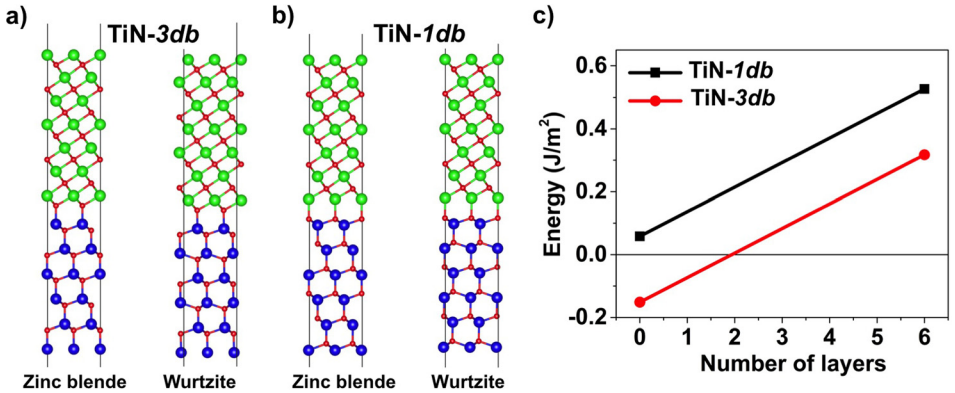

FIG. 6. Atomic structure of AlN/TiN slabs (a) TiN-3*db* and (b) TiN-1*db*. (c) Relative stability of *zb*-AlN with respect to *wz*-AlN as a function of number of layers.

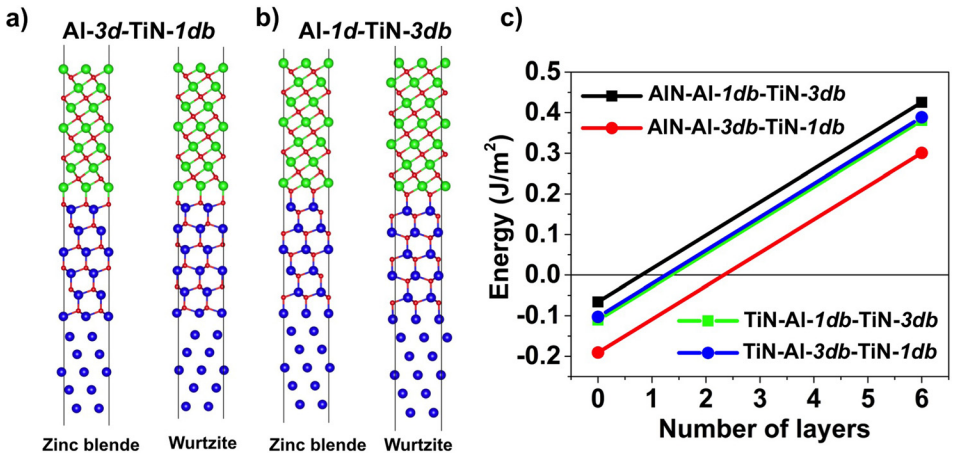

FIG. 7. Atomic structure of AlN/TiN slabs (a) Al-1 *d*-TiN-3 *d* and (b) Al-3 *d*-TiN-1 *d*. (c) Relative stability of *zb*-AlN with respect to *wz*-AlN as a function of number of layers.

TABLE II. Relative interface energy calculated for various configurations at in-plane lattice parameter of TiN and *zb*-AlN. For comparison, the relative interface energy of Al/AlN and AlN/TiN and their sum (Al/AlN + AlN/TiN) are also listed.

In-plane lattice parameter	Configurations	Al/AlN E_{int}^{rel} (J/m^2)	AlN/TiN E_{int}^{rel} (J/m^2)	Sum of Al/AlN and AlN/TiN E_{int}^{rel} (J/m^2)	Al/AlN/TiN E_{int}^{rel} (J/m^2)
TiN	Al-1*db*-TiN-3*db*	−0.210	0.092	−0.118	−0.111
	Al-3*db*-TiN-1*db*	0.010	−0.132	−0.122	−0.103
zb-AlN	Al-1*db*-TiN-3*db*	−0.109	0.058	−0.051	−0.066
	Al-3*db*-TiN-1*db*	−0.058	−0.151	−0.209	−0.182

bilayer Al/AlN and AlN/TiN interfaces. Table II summarizes the results of the relative interface energy of various configurations of Al/AlN/TiN interfaces at the in-plane lattice parameters corresponding to the equilibrium lattice parameter of TiN and *zb*-AlN. Also tabulated is the relative interface energy of Al/AlN and AlN/TiN and their sum (Al/AlN + AlN/TiN). The maximum difference in the relative interface energies calculated using two methods is 0.03 J/m^2. This relatively small difference confirms that the assumption we made in the calculation of the relative interface energy of Al/AlN and AlN/TiN bilayers that free surface energy of *zb*-AlN and *wz*-AlN is the same and is approximately right.

D. Nitridation of Al to AlN

Now we explore the possibility of formation of *zb*-AlN by the sequential filling of N interstitials in fcc Al matrix. In Fig. 8(a), a schematic shows the Al (111) surface and various positions where nitrogen atoms can be absorbed or adsorbed. These include the tetrahedral and octahedral interstitials and on-top positions. We started by calculating the formation energy of these various positions and found that only tetrahedral and octahedral interstitial positions are stable positions.

The tetrahedral N interstitials would lead to the formation of *zb*-AlN, while octahedral N interstitials would lead to the formation of *rs*-AlN. Figs. 8(b) and 8(c) show a sequential filling of N interstitials at (b) tetrahedral and (c) octahedral positions, up to four N atoms. In Fig. 8(d), the formation energies of these small cluster precursors to the two nitride phases are plotted as tetrahedral and octahedral positions and are filled by nitrogen atoms in two cases: one case close to the free Al(111) surfaces and the other case in bulk Al. It is

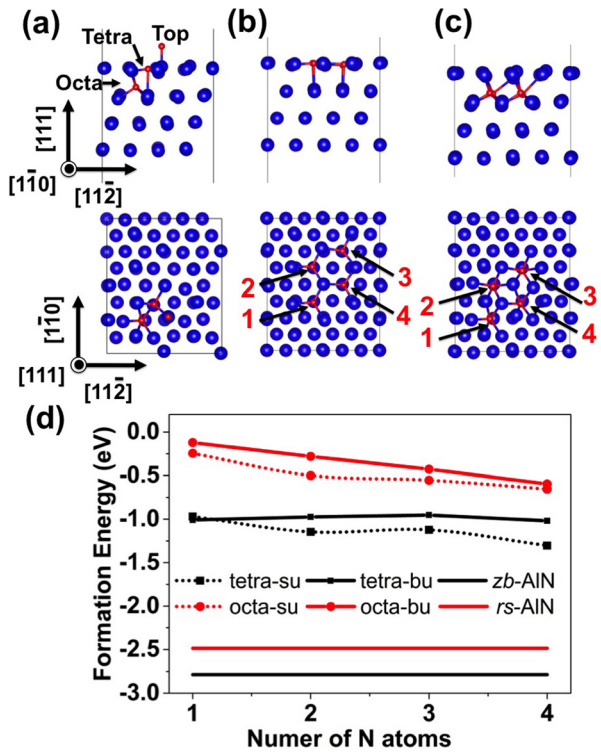

FIG. 8. (a) Various initial positions (on-top, octahedral interstitials, tetrahedral interstitials) considered when Al is exposed to nitrogen. Sequential filling of (b) tetrahedral and (c) octahedral positions, top row and bottom row are side and top views of the slab. (d) Formation energy of N interstitials per nitrogen as tetrahedral (tetra) and octahedral (octa) positions are filled close to the free surface (symbol su) and in bulk (symbol bu) calculated, and formation energy of bulk AlN in zincblende (zb-AlN) and rocksalt phases (rs-AlN).

clear that N interstitials occupying tetrahedral position is always energetically favorable compared to the octahedral position in these cases. We note that, at the lattice constant of Al, bulk *rs*-AlN phase actually is lower in energy than that of highly strained bulk *zb*-AlN, since *rs*-AlN has a lattice constant close to that of Al. However, the preference of nitrogen atoms to sit at the tetrahedral positions in Al thus favors the formation of *zb*-AlN compared to *rs*-AlN. In earlier Subsections III B and III C, we already show the DFT results on the energetics of Al/AlN, AlN/TiN, or Al/AlN/TiN multilayers, the experimentally observed zincblende layers cannot be stabilized via interface thermodynamics. Thus, the formation of a zinc-blende AlN thin film is determined to be a kinetically driven process rather than a thermodynamically driven process. The zinc blende AlN grows to the thickness of 1.5 nm only; this may be due to the self-limiting effect of N diffusion into Al. As AlN grows in thickness, it becomes harder for N to diffuse further into Al layer, thus limiting the thickness of AlN to 1.5 nm.

IV. CONCLUSION

In summary, using *ab initio* DFT, an unusual growth mechanism of metastable zincblende AlN thin film by diffusion of nitrogen atoms into Al lattice is established. All results presented in the manuscript are at 0 K, but this should not dramatically effect conclusions as experimental conditions for growth of film is at room temperature. We studied the thermodynamic stability of AlN as zincblende phase due to the various epitaxial strains and found that the energy of zincblende phase is always higher than that of the wurtzite phase. We then studied the relative stability of Al/AlN and AlN/TiN bilayer interfaces, and Al/AlN/TiN multilayers when AlN is in the zincblende versus in the wurtzite phases. For all configurations considered, the maximum number of *zb*-AlN layers that interfaces can stabilize is about two, while there are approximately six layers of *zb*-AlN layers during the growth in experimental conditions. The DFT results suggest that the interface effect by a thermodynamically driven process cannot explain the formation of zincblende AlN observed. We then compared the formation energetics of the rocksalt and the zincblende AlN in fcc Al through direct diffusion of nitrogen atoms to Al octahedral and tetrahedral interstitials. The preference of nitrogen atoms to sit at the tetrahedral positions in Al favors the formation of *zb*-AlN compared to *rs*-AlN. Thus, the formation of zinc-blende AlN thin film is determined to be a kinetically driven process.

ACKNOWLEDGMENTS

The authors thank Nan Li for the helpful discussions. This work was supported by the U.S. Department of Energy, Office of Science, and Office of Basic Energy Sciences.

[1]A. Madan, I. W. Kim, S. C. Cheng, P. Yashar, V. P. Dravid, and S. A. Barnett, Phys. Rev. Lett. **78**, 1743 (1997).
[2]C.-M. Lin, W.-C. Lien, V. V. Felmetsger, M. A. Hopcroft, D. G. Senesky, and A. P. Pisano, Appl. Phys. Lett. **97**, 141907 (2010).
[3]A. Ababneh, M. Alsumady, H. Seidel, T. Manzaneque, J. Hernando-Garcia, J. L. Sanchez-Rojas, A. Bittner, and U. Schmid, Appl. Surf. Sci. **259**, 59 (2012).
[4]N. E. Christensen and I. Gorczyca, Phys. Rev. B **47**, 4307 (1993).
[5]N. E. Christensen and I. Gorczyca, Phys. Rev. B **50**, 4397 (1994).
[6]A. Siegel, K. Parlinski, and U. D. Wdowik, Phys. Rev. B **74**, 104116 (2006).
[7]I. Petrov, E. Mojab, R. C. Powell, J. E. Greene, L. Hultman, and J. E. Sundgren, Appl. Phys. Lett. **60**, 2491 (1992).
[8]I. W. Kim, Q. Li, L. D. Marks, and S. A. Barnett, Appl. Phys. Lett. **78**, 892 (2001).
[9]Q. Li, I. W. Kim, S. A. Barnett, and L. D. Marks, J. Mater. Res. **17**, 1224 (2002).
[10]I. W. Kim, A. Madan, M. W. Guruz, V. P. Dravid, and S. A. Barnett, J. Vac. Sci. Technol., A **19**, 2069 (2001).
[11]C. Stampfl and A. J. Freeman, Appl. Surf. Sci. **258**, 5638 (2012).
[12]V. I. Ivashchenko, S. Veprek, P. E. A. Turchi, V. I. Shevchenko, J. Leszczynski, L. Gorb, and F. Hill, Thin Solid Films **564**, 284 (2014).
[13]N. Li, S. K. Yadav, J. Wang, X. Y. Liu, and A. Misra, Sci. Rep. **5**, 18554 (2015).
[14]G. Kresse and J. Hafner, Phys. Rev. B **47**, 558 (1993).
[15]G. Kresse and J. Furthmuller, Comput. Mater. Sci. **6**, 15 (1996).
[16]J. P. Perdew, K. Burke, and M. Ernzerhof, Phys. Rev. Lett. **77**, 3865 (1996).
[17]P. E. Blochl, Phys. Rev. B **50**, 17953 (1994).
[18]S. K. Yadav, R. Ramprasad, A. Misra, and X. Y. Liu, J. Appl. Phys. **111**, 083505 (2012).
[19]S. K. Yadav, R. Ramprasad, A. Misra, and X. Y. Liu, Acta Mater. **74**, 268 (2014).
[20]C. Kittle, *Introduction to Solid State Physics* (Wiley, New York, 1986).
[21]H. Schulz and K. H. Thiemann, Solid State Commun. **23**, 815 (1977).
[22]N. Schonberg, Acta Chem. Scand. **8**, 199 (1954).
[23]G. N. Kamm and G. A. Alers, J. Appl. Phys. **35**, 327 (1964).
[24]L. E. Mcneil, M. Grimsditch, and R. H. French, J. Am. Ceram. Soc. **76**, 1132 (1993).
[25]M. Ueno, A. Onodera, O. Shimomura, and K. Takemura, Phys. Rev. B **45**, 10123 (1992).
[26]I. Yonenaga, T. Shima, and M. H. F. Sluiter, Jpn. J. Appl. Phys., Part 1 **41**, 4620 (2002).
[27]J. O. Kim, J. D. Achenbach, P. B. Mirkarimi, M. Shinn, and S. A. Barnett, J. Appl. Phys. **72**, 1805 (1992).
[28]J. Neugebauer and M. Scheffler, Phys. Rev. B **46**, 16067 (1992).
[29]S. K. Yadav, R. Ramprasad, J. Wang, A. Misra, and X. Y. Liu, Modell. Simul. Mater. Sci. Eng. **22**, 035020 (2014).
[30]D. Bhattacharyya, X. Y. Liu, A. Genc, H. L. Fraser, R. G. Hoagland, and A. Misra, Appl. Phys. Lett. **96**, 093113 (2010).
[31]H. Vollstadt, E. Ito, M. Akaishi, S.-I. Akimoto, and O. Fukunaga, Proc. Jpn. Acad., Ser. B **66**, 7 (1990).
[32]P. E. Vancamp, V. E. Vandoren, and J. T. Devreese, Phys. Rev. B **44**, 9056 (1991).
[33]S. B. Zhang and S. H. Wei, Phys. Rev. Lett. **92**, 086102 (2004).